ARTICLE

Aberrant photoelectric effect in the topological insulator/n-GaN heterojunction (Bi_2Te_3/n-GaN) under unpolarized illumination

Received 00th January 20xx,
Accepted 00th January 20xx

DOI: 10.1039/x0xx00000x

Faizan Ahmad, [a] Kavindra Kandpal [b], Roshani Singh [c], Rachana Kumar[d] and Pramod Kumar *[c]

1. Fabrication flow process diagram

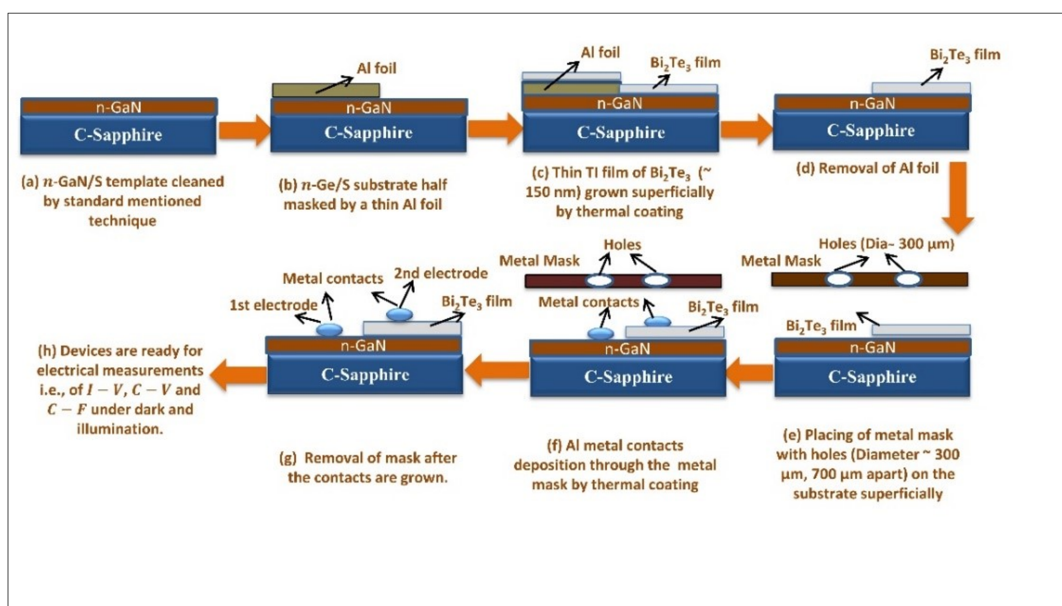

Figure S1 Flow diagram depicting the steps involved in the fabrication process of Bi_2Te_3/n-GaN heterostructure.

[a] Electrical, Computer and Energy Engineering, Arizona State University, Tempe, AZ-85281, United States. Email: faizanash1986@gmail.com
[b] Department of Electronics and Communication Engineering, IIIT-Allahabad, Prayagraj, 211012, India
[c] Spintronics and Magnetic Materials Laboratory, Department of Applied Sciences, IIIT-Allahabad, Prayagraj, 211012, India. E-mail: pkumar@iiita.ac.in
[d] ASSIST Division,CSIR-Indian Institute of Toxicology Research, Lucknow, Uttar Pradesh, India-226024.

† No conflict of interest from any of the authors.

Electronic Supplementary Information (ESI) available: [details of any supplementary information available should be included here]. See DOI: 10.1039/x0xx00000x

Please do not adjust margins

2. Material and microstructure study of the Bi_2Te_3 TI film grown on n-GaN Substrate

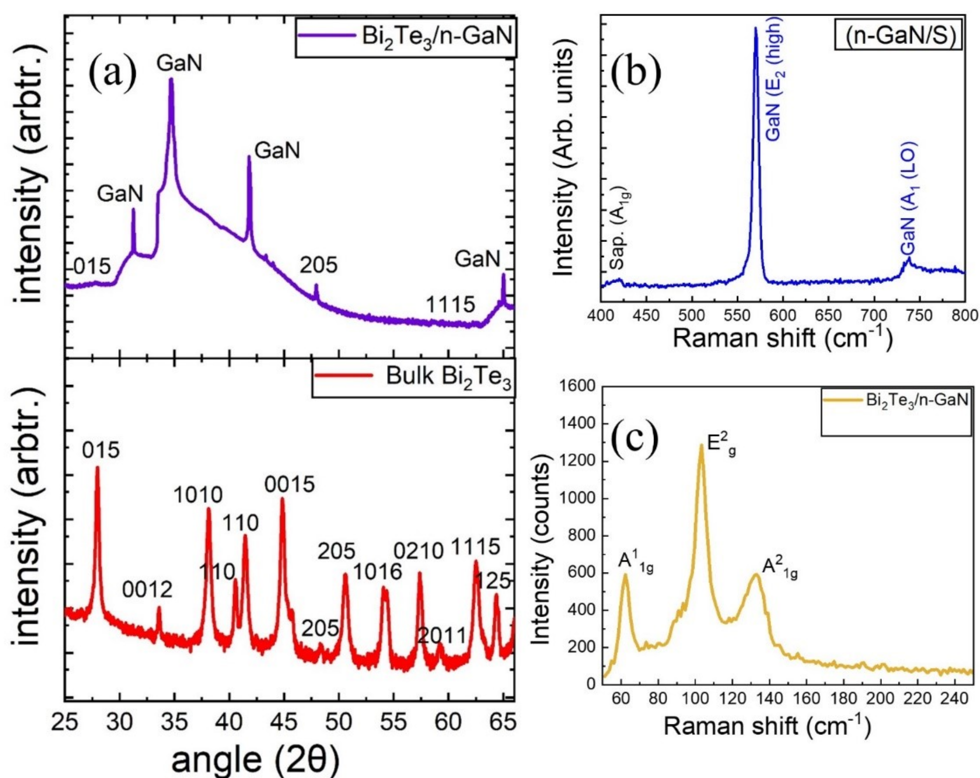

Figure S2 (a) Shows the result of XRD of Bi_2Te_3/n-GaN/S and the bulk Bi_2Te_3 (b) Shows the Raman spectroscopy results of n-GaN/S (c) Shows the Raman spectroscopy results of n-GaN/Bi_2Te_3/S.

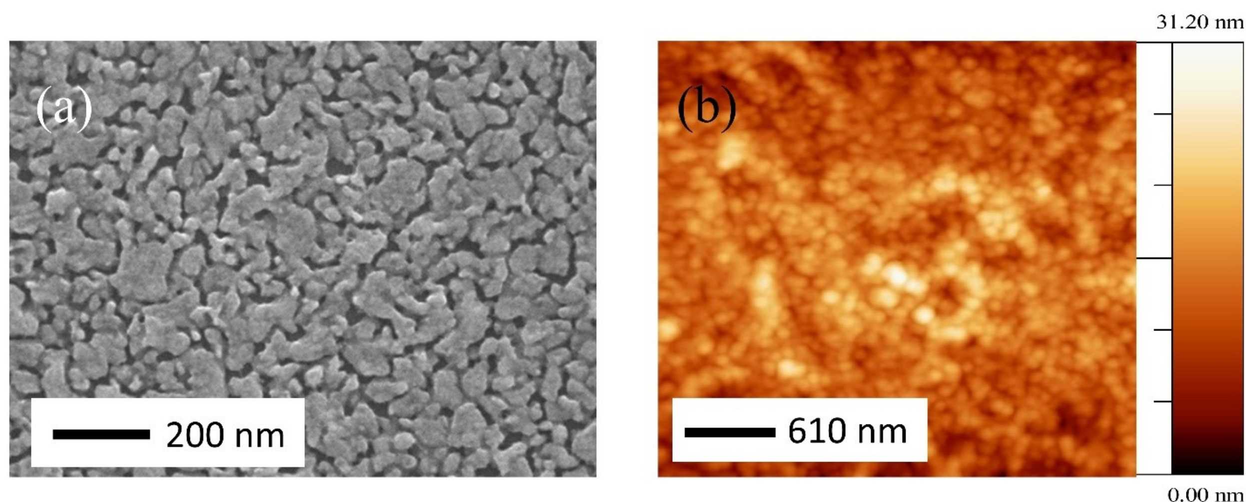

Figure S3 shows the SEM image of the grown Bi_2Te_3 film grown on n-GaN/S (b) Shows the AFM micrograph of the Bi_2Te_3 TI film on n-GaN/S substrate.

This journal is © The Royal Society of Chemistry 20xx

Please do not adjust margins

Figure S2a shows the XRD results of Bi_2Te_3 TI film grown on n-GaN template (sapphire). XRD peak of Bi_2Te_3 TI film in the Bi_2Te_3/n-GaN heterostructure revealed the polycrystalline rhombohedral structure [space group R-3m (166)]. The XRD peaks obtained conforms with the results of the bulk Bi_2Te_3 compound. The peaks were being matched with the standard International Center for diffraction Data (ICDD) having Portable Document Format (PDF) card No. 00-002-0524. Raman spectroscopy for n-GaN/Sapphire(S) template (Figure S2c), showed the peak of strong E_2 transverse optical (TO) mode and A_1 longitudinal optical (LO) modes observed at 570 cm^{-1} and 738 cm^{-1} with a little shifting of the A_1 (LO) mode for the n-GaN/S as observed earlier[1]. The small peak of the sapphire substrate was obtained at 420 cm^{-1} representing the A_{1g} active mode which was found consistent with the earlier results[2]. For the Bi_2Te_3/n-GaN heterostructure peaks at 62.3 cm^{-1}, 103.3 cm^{-1}, and 133.0 cm^{-1} were obtained representing the A^1_{1g} (LO), E^2_g(TO), and A^2_{1g} (LO) active modes. The peaks obtained were sharp and quite similar to the previous results of grown Bi_2Te_3 film on GaN[3]. A little shifting in the wavenumber of the peaks was seen which may be due to a small defect during the grown process of the Bi_2Te_3 film[3]. Figure S3a shows the SEM micrograph image of the Bi_2Te_3 film on the GaN/S template, confirming the porosity of the film with the size of the grain between the range ~ 70-80 nm. AFM image of the Bi_2Te_3 film on GaN/S template in Figure S3b, revealed the root mean square roughness (RMS) = 3.8088 nm and average roughness = 3.7908. The RMS roughness revealed the uniformity of the film which is a requisite for optimum conductivity and good performance of the devices. Small surface roughness also ascertains the minimum interface state density (D_{it})[4] at the contact junction with the Bi_2Te_3 film which is suitable for the device. The porous nature of the film, observed from the SEM image was due to the growth process of Thermal coating[5].

3. $I-V$ study of the Bi_2Te_3/n-GaN heterojunction and the Bi_2Te_3 TI film

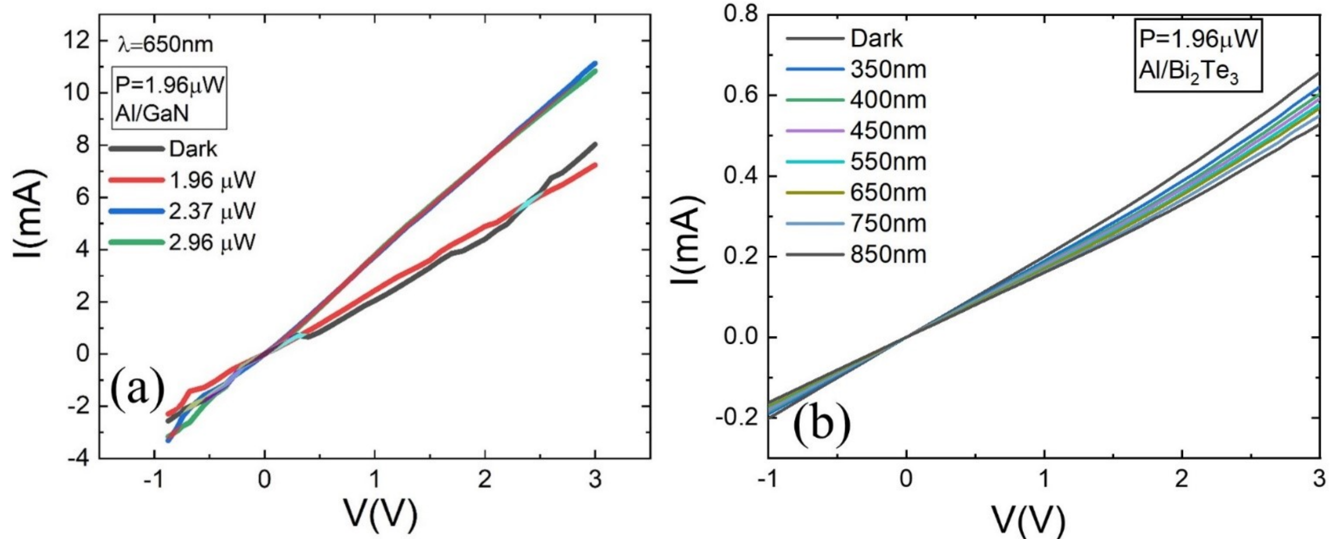

Figure S4 (a) shows the $I-V$ results obtained through Al metallic contacts on the n-GaN template which was observed to be ohmic and conducting in both positive and negative biasing for wavelength (λ = 650 nm) and incident power (P at 1.96 μW, 2.37 μW and 1.96 μW) (b) $I-V$ results measured through the Al metal contacts on the Bi_2Te_3 TI film grown on the n-GaN template, under the dark and illumination conditions for λ varied from 350 nm to 950 nm, at P= 1.96 μW.

We annealed the devices Bi_2Te_3/n-GaN after the contact deposition in the range of 200-300 °C for 1- 2 h to ensure the ohmic contacts. Figure S4a shows the results in both the positive and negative biasing in opposite quadrant which confirmed the ohmic behaviour and exclude the depletion layer affect. The results in Figure S4a showed the consistent results obtained for wavelength (λ)= 650 nm and incident power (P) at 1.96 µW, 2.37 µW and 1.96 µW.

4. Semi log (I-V) and plot Extraction of ideality factor

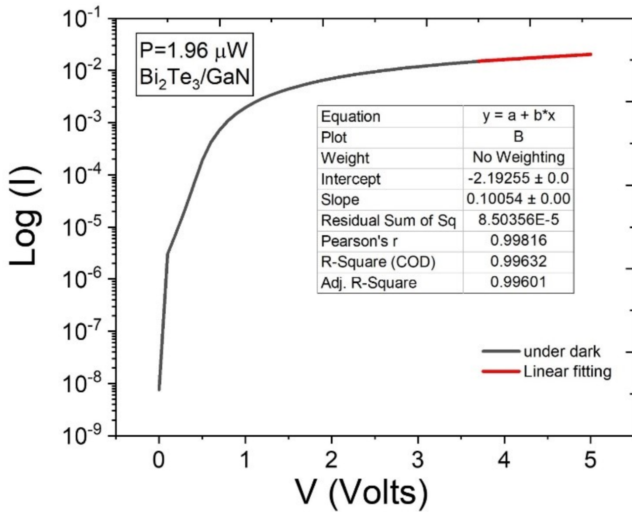

Figure S5 Shows the Semi-log (I-V) plot and its linear fitting in the saturation region.

In forward-bias, $I-V$ characteristics of a diode is given by the Eq. S1 as:

$$I = I_R(e^{\frac{qV}{nkT}} - 1) \quad \text{(S1)}$$

I_R is the reverse saturation current

k is the Boltzmann constant

T is the temperature in Kelvin, q is the electronic charge

Assuming $V \gg \frac{kT}{q}$ (Thermal Voltage) the Eq. 1 can be

$$n \cong \frac{q}{kT}\frac{1}{\frac{dV}{d(\ln I)}} \quad \text{(S2)}$$

Calculating from the Eq. S2 by taking the slope of the Semi-log (I-V) characteristics (Figure S5) at the saturation voltage we get the ideality factor as n ≈3.88.

5. 2-Diode Simulation for extracting the n-GaN/Bi_2Te_3 heterojunction device parameters under the dark and illumination conditions

The experimental $I-V$ results of the Bi_2Te_3/n-GaN heterojunction were used for simulating by 2-diode model[6],[7]. $I-V$ characteristics of solar cell heterojunction devices are represented by a single diode, but more circuit elements are required to study the behaviour in a much more precise way, which requires a 2-diode circuit model[6,7] which is shown in Figure S6. In Figure S6, $J(V)$ and V represents the current and voltage at the contacts. R_{pp}, R_{ss} are the ohmic parallel and series resistance included in junction devices[7], representing all the contributing currents i.e. diffusion, recombination, and ohmic[7]. The diode D_{01} represents the diffusion current $J_d(V)$, D_{02} represents the recombination current $J_r(V)$, in the depletion region[8]. J_{ph} is the photocurrent in the circuit (J_{ph})[8] which is assumed zero because of the dark conditions of measurements. Therefore, the dark current represented by the 2-diode model Equation (S1)[8]: -

$$J(V) = J_{01}\left(e^{\frac{qV}{n_1kT}} - 1\right) + J_{02}\left(e^{\frac{qV}{n_2kT}} - 1\right) = J_d(V) + J_r(V)$$

(S1)

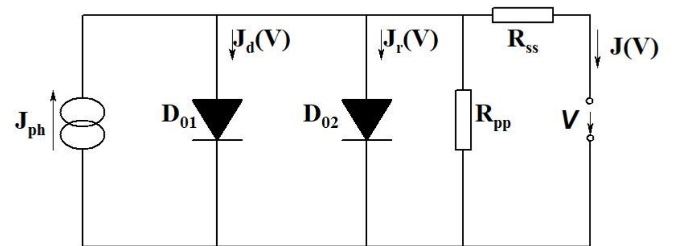

Figure S6 An equivalent 2-diode model circuit[6] was used for the simulation of the n-GaN/Bi_2Te_3 heterojunctions under dark and illuminated conditions at room temperature (300 K).

Please do not adjust margins

J_{01} and J_{02} is the pre-exponential coefficient of $J_d(V)$ and $J_r(V)$. J_{01} is the recombination current occurring in the bulk, dominant usually at higher bias[8] J_{02} denotes the saturation current density due to depletion region recombination at the junction which is dominant at lower bias[8]. n_1, n_2 is the ideality factor for the diode $D_{01}$and D_{02} [8,6].The ideal value of n_1 is 1, if the carrier lifetime is independent of the minority carrier concentration[9]. The ideal value of n_2 is 2[9]. The 2-diode model was used to fit and extract find out various parameters such as J_{01}, J_{02}, n_1, n_2, R_{pp} and R_{ss}[7]. Current here is expressed as current densities, which makes it independent of the cell area. R_{ss} is also expressed in $\Omega - cm^2$. Our device's area is 0.0049 cm^2, which is the area between the consecutive Al contacts (Figure 1 in the manuscript). The simulated parameters give insight into the recombination of charge carriers as well as about the efficiency of Bi_2Te_3/n-GaN heterojunction devices when employed in electronics devices, particularly in solar cells[10]. The efficiency of solar cell devices was seen to be limited due to the various recombination of electrons such as depletion-region recombination, edge recombination, and resistance-limited recombination, as seen in previous studies [9]. Figure S7a shows the Current density-Voltage ($J - V$) and the local ideality factor ($n - V$) plot obtained by the 2-diode simulation fitting for the experimental $I - V$ results of the Bi_2Te_3/n-GaN heterojunction under the dark conditions. Whereas the individual characteristics for the D_{01}, D_{02} diodes, series resistance (R_{ss}) and parallel resistance R_{pp} is also shown, as obtained from the fittings. The $J - V$ well fitted with the experimental results obtained with the ideality factor obtained as $n = 3.0138$. Figure S7b & S7c shows the series resistance (R_{ss}) and parallel resistance R_{pp} shows almost the same decreasing behavior with the increase in the incident photon energy of the light. This represents the behavior of the Bi_2Te_3/n-GaN heterojunction devices after the illumination where the series resistance decreases with the increase in the incident photon energy of the light. This behavior was also evident from the $I - V$ characteristics of the Bi_2Te_3/n-GaN heterojunction devices at constant incident power (Figure 2 in the Manuscript).

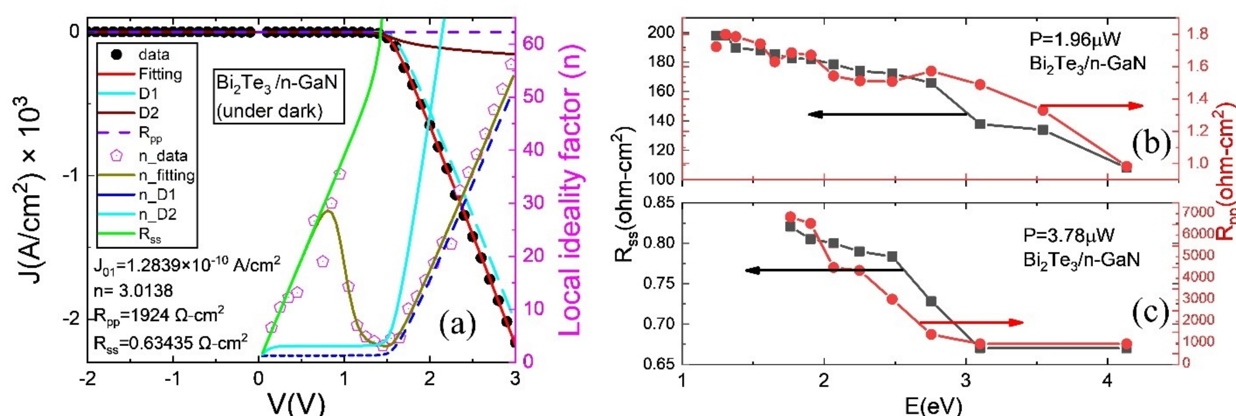

Figure S7 (a) Shows the current density-voltage ($J - V$) and the local ideality factor ($n - V$) plot obtained by the 2-diode simulation fitting for the experimental $I - V$ results of the Bi_2Te_3/n-GaN heterojunction under the dark conditions with individual characteristics for the D_{01}, D_{02} diodes and parallel resistance R_{pp} (b) Shows the series resistance (R_{ss}) the parallel resistance (R_{pp}) plot versus the incident light energy (E) for the Bi_2Te_3/n-GaN heterojunction under illumination at the incident power of (b) 1.96 μW and (c) for 3.78 μW

Please do not adjust margins

Please do not adjust margins

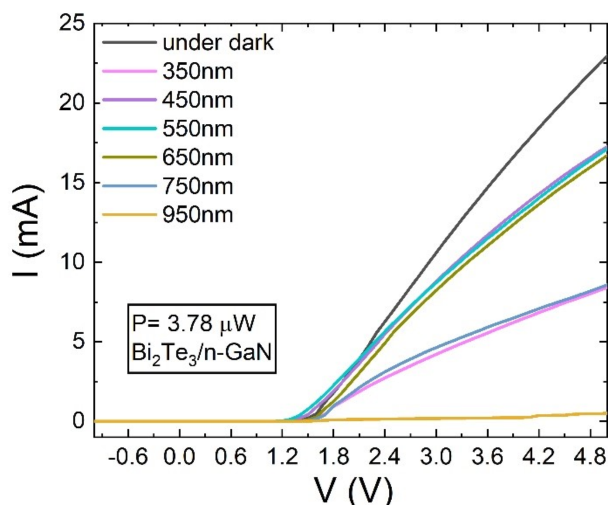

Figure S8 Shows the $I-V$ characteristics for the Bi_2Te_3/n-GaN heterojunction device under the dark and illumination conditions when the wavelength of the incident light was varied from 350 nm to 950 nm under the constant incident light power of 3.78 μW

Figure S9 (a) Shows the $I-V$ characteristics measured through the Al contacts on the Bi_2Te_3 TI film on n-GaN template at a constant incident light of wavelength (λ) = 650 nm with power (P) varying from 1.96 μW- 3.78 μW

 This journal is © The Royal Society of Chemistry 20xx

Please do not adjust margins

Please do not adjust margins

(b) shows the contour plot of current-voltage $(I-V)$ versus the incident photon light energy (E) in eV at a constant power of 1.96 μW (c) shows the contour plot of energy-responsivity $(E-R)$ versus the bias voltage (V) measured through the Al contacts, at constant 1.96 μW incident power (d) The energy-detectivity $(E-D)$ versus the bias voltage (V) plot measured through the Al contacts at 1.96 μW incident power.

5. Capacitance-frequency ($C-f$), (G_p/ω-ω) plot under dark and illumination and optical parameters measurements

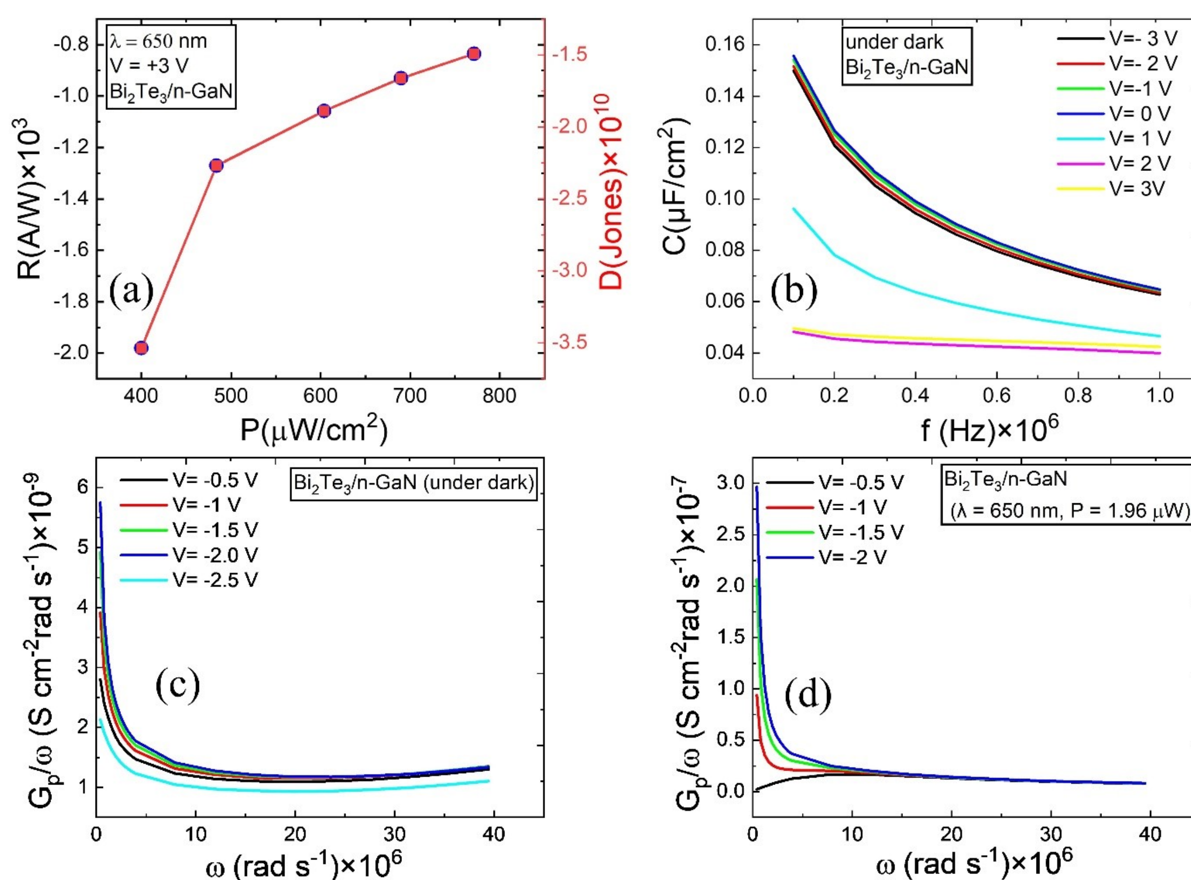

Figure S10 (a) Responsivity-power density ($R-P_D$) plot (in blue) and detectivity-power density ($D-P_D$) (in red) at a constant bias voltage of 3 V and wavelength of the incident light (λ) = 650 nm for the Bi_2Te_3/n-GaN heterojunction device (b) The Capacitance-frequency ($C-f$) plot for the Bi_2Te_3/n-GaN heterojunction with the bias voltage range from -3 V to +3 V (at +1 V interval), under the dark conditions (c) conductance/radial frequency (G_p/ω) versus radial frequency (ω) plot, for Bi_2Te_3/n-GaN heterojunction, measured for bias voltage from -2 V to 0 V (at interval of 0.5 V) under the dark conditions (d) (G_p/ω - ω) plot for the Bi_2Te_3/n-GaN heterojunction, measured for range of bias voltage from -2 V to -0.5 V (interval of 0.5 V) under the the presence of light ($\lambda =$ 650 nm, P =1.96 μW).

7. Ultrafast Dynamics of Bi_2Te_3/n-GaN heterojunction and the Bi_2Te_3 TI film

We have performed the ultrafast dynamics in Bi_2Te_3 films and its heterojunction with n-GaN. In nascent film on excitation with 410nm pump wavelength, a transient absorption in visible region stands appearing after 1.8ps

Please do not adjust margins

Please do not adjust margins

with maxima at ~540nm and other small transient bands at ~710nm and 750nm. The transient absorption starts disappearing with appearance of ground state belching in the range of 550nm to 800nm. The GSB appears at ~623nm and 764nm. The lifetime are presented in the Table 2. In NIR region after ~1.1ps time delay broad GSB is observed between 900nm to 1600nm with maxima ~1155nm which sifted to ~1340nm with delay.

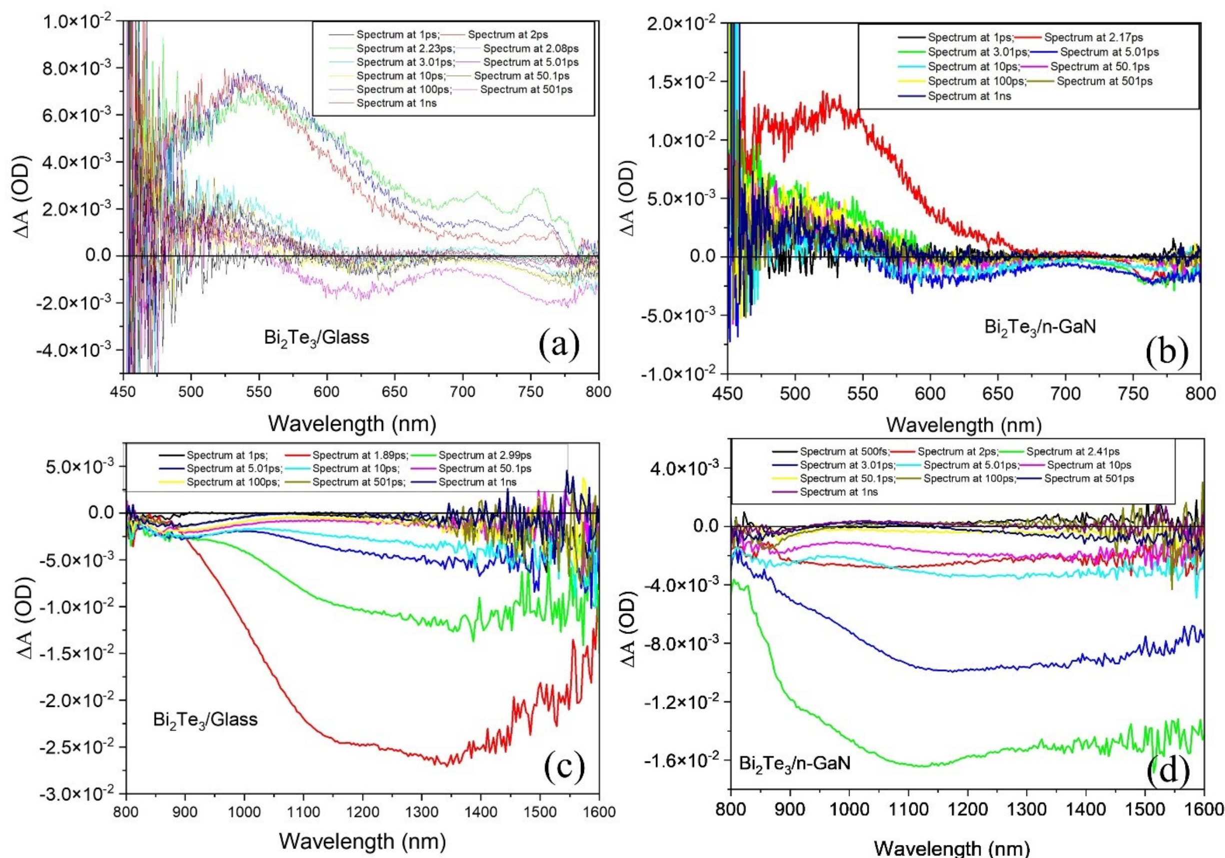

Figure S11. Transient absorption (TA) spectra showing the amplitude variation (ΔA) vs. wavelength (nm) plot in the visible range (450 nm-800 nm) for (a) Glass/Bi_2Te_3 heterojunction (b) n-GaN/Bi_2Te_3 heterojunction. (c&d) Shows the (ΔA) vs. wavelength (nm) plot in the near-infrared (NIR) range (800 nm-1600 nm) at different time delays for (c) Glass/Bi_2Te_3 heterojunction (d) n-GaN/Bi_2Te_3 heterojunction.

This journal is © The Royal Society of Chemistry 20xx

Please do not adjust margins

Please do not adjust margins

Table S1. Summary of the various parameters derived from the Glass/Bi_2Te_3 and n-GaN/Bi_2Te_3 transient absorption (TA) spectra and fitting on the TA results

Bi_2Te_3 Film					**GaN/Bi_2Te_3 Heterojunction**			
S.N.	Wavelength(λ) (nm)	E(ev) =1240/λ	τ_1(ps)	τ_2(ps)	Wavelength (λ) (nm)	E(ev) =1240/λ	τ_1(ps)	τ_2(ps)
1	540 (TA)1	2.296	1.07	-	532 (TA)1	2.331	0.6	-
2	710 (TA)1	1.746	0.73	6.4	758 (GSB)	1.636	15.8	-
3	750 (TA)1	1.653	5.7	1.57	775 (GSB)	1.600	22	-
4	623 (GSB)3	1.990	13.6	-	610 (GSB)3	2.033	11.2	-
5	764 (GSB)2	1.623	9.45	-	762 (GSB)2	1.627	2.5	-
6	1155 (GSB)4	1.074	0.78	11.7	1100 (GSB)4	1.127	0.62	10.2
7	1340 (GSB)4	0.925	0.76	14.9	-		-	-

Please do not adjust margins

Please do not adjust margins

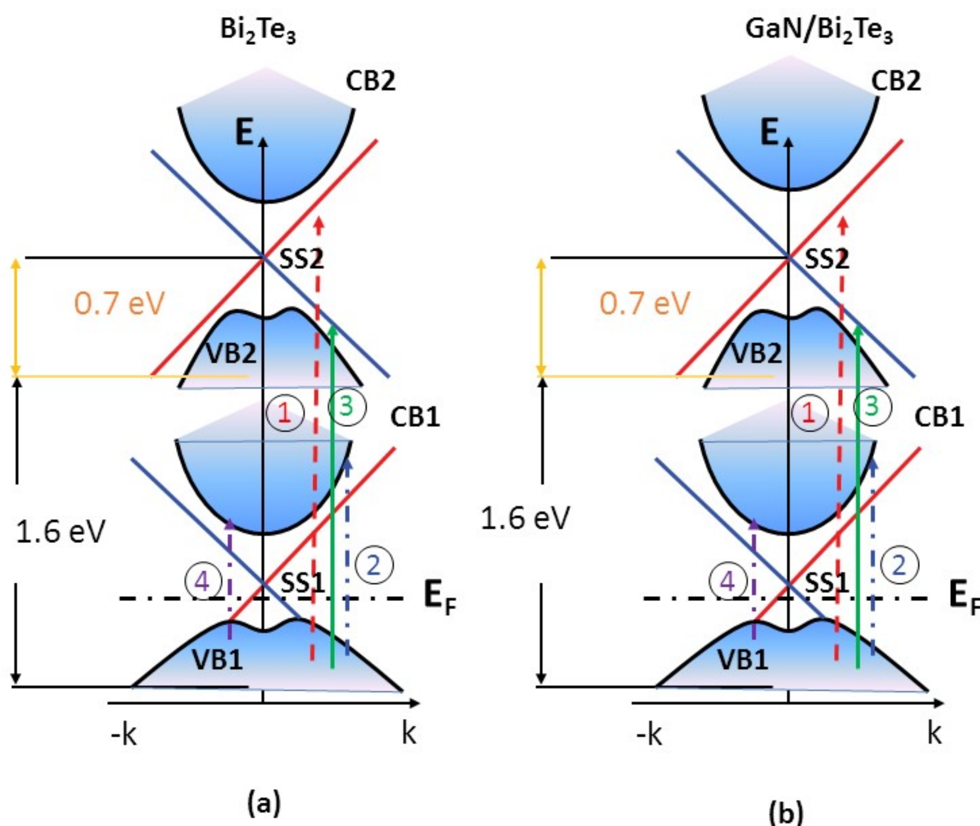

Figure S12. Shows the transition of the spin-oriented charge carriers between the different conducting states such as SS1 to SS2, CB1 to SS2, VB1 to SS1, and SS1 to CB2 respectively for (a) Glass/Bi_2Te_3 (b) n-GaN/Bi_2Te_3 heterojunction. The SS1, SS2 representing the two surface states, CB1, CB2 are the first and the second conduction band, VB1, VB2 first, and the second valence band.

In visible region, TA appears after 1.8ps delay time with maxima ~523nm along with two GSB at 758nm and 775nm. These two GSB merges and new GSB appears at 610nm and 762nm after 5ps delay time. In NIR region, the GSB appears after ~1.8ps delay time with maxima ~1100nm and fits bi-exponentially. However, it's similar to Glass/Bi_2Te_3, in the heterojunction no GSB appears 1300nm range.

For the wavelength in the excitation range of 350 nm to 950 nm transition of the Bi_2Te_3/n-GaN heterojunction from the first surface states (SS1) to the second surface states (SS2), the transition from the first conduction band (CB1) to the second surface state (SS2), and that from the first valence band (VB1) to the SS1, VB1 to VB2 and charge transfer from CB of GaN to CB of Bi_2Te_3 forming charge transfer (CT)[11] state are possible[12]. But there is no visible CT state present here (Figure S12). The Dirac point of SS2 is located above the Dirac point of SS1.[12,13,14,15–18] The spin-polarized electrons in n-GaN will inject into Bi_2Te_3 film, and injected spin-up electrons will recombine with holes in the VB1. Therefore, the hole concentration from the bottom of the Bi_2Te_3 film get suppressed and reduces the total current contribution. Since, the total current is due to the contribution of the top and the bottom surface of the Bi_2Te_3 film i.e., the $I_{e1}$and I_{e2}. The suppression of the bottom surface of the current contribution enhances the total contribution of the Bi_2Te_3 film in the total current.

5. References

1 A. Hushur, M. H. Manghnani and J. Narayan, *J. Appl. Phys.*, 2009, **106**, 54317.

2 J. Thapa, B. Liu, S. D. Woodruff, B. T. Chorpening and M. P. Buric, *Appl. Opt.*, 2017, **56**, 8598–8606.

3 H. Xu, Y. Song, Q. Gong, W. Pan, X. Wu and S. Wang, *Mod. Phys. Lett. B*, 2015, **29**, 1550075.

4 S. Kasap and P. Capper, *Springer handbook of electronic and photonic materials*, Springer,

This journal is © The Royal Society of Chemistry 20xx

Please do not adjust margins

Please do not adjust margins

2017.

5 F. Ahmad, K. Kandpal, N. Kumar, R. Kumar and P. Kumar, *IEEE Trans. Electron Devices*.

6 S. Suckow, .

7 O. Breitenstein and S. Rißland, *Sol. Energy Mater. Sol. Cells*, 2013, **110**, 77–86.

8 O. Breitenstein, *Sol. Energy Mater. Sol. Cells*, 2011, **95**, 2933–2936.

9 O. Breitenstein, J. Bauer, P. P. Altermatt and K. Ramspeck, *Solid State Phenom.*, 2009, **156–158**, 1–10.

10 U. Stutenbaeumer and B. Mesfin, *Renew. Energy*, 1999, **18**, 501–512.

11 F. Ahmad, R. Kumar, S. S. Kushvaha, M. Kumar and P. Kumar, *npj 2D Mater. Appl.*, 2022, **6**, 12.

12 C.-M. Tu, T.-T. Yeh, W.-Y. Tzeng, Y.-R. Chen, H.-J. Chen, S.-A. Ku, C.-W. Luo, J.-Y. Lin, K.-H. Wu and J.-Y. Juang, *Sci. Rep.*, 2015, **5**, 1–8.

13 M. C. Wang, S. Qiao, Z. Jiang, S. N. Luo and J. Qi, *Phys. Rev. Lett.*, 2016, **116**, 36601.

14 Y. Q. Huang, Y. X. Song, S. M. Wang, I. A. Buyanova and W. M. Chen, *Nat. Commun.*, 2017, **8**, 15401.

15 H.-H. Kung, A. P. Goyal, D. L. Maslov, X. Wang, A. Lee, A. F. Kemper, S.-W. Cheong and G. Blumberg, *Proc. Natl. Acad. Sci.*, 2019, **116**, 4006–4011.

16 J. A. Sobota, S.-L. Yang, A. F. Kemper, J. J. Lee, F. T. Schmitt, W. Li, R. G. Moore, J. G. Analytis, I. R. Fisher and P. S. Kirchmann, *Phys. Rev. Lett.*, 2013, **111**, 136802.

17 H. Soifer, A. Gauthier, A. F. Kemper, C. R. Rotundu, S.-L. Yang, H. Xiong, D. Lu, M. Hashimoto, P. S. Kirchmann and J. A. Sobota, *Phys. Rev. Lett.*, 2019, **122**, 167401.

18 W. P. Fernandes, A. de Siervo and E. A. Soares, .

Please do not adjust margins